Published in final edited form as:
Biomaterials. 2010 November ; 31(32): 8235–8244. doi:10.1016/j.biomaterials.2010.07.034.

Pericyte-Based Human Tissue Engineered Vascular Grafts

Wei He, PhD[1,5,6], **Alejandro Nieponice, MD, PhD**[1,5,6], **Lorenzo Soletti, PhD**[1,2,5,6], **Yi Hong, PhD**[1,5,6], **Burhan Gharaibeh, PhD**[3,4,5], **Mihaela Crisan, PhD**[3,4], **Arvydas Usas, MD**[3,4], **Bruno Peault, PhD**[3,4,5], **Johnny Huard, PhD**[3,4,5], **William R. Wagner, PhD**[1,2,5,6], and **David A. Vorp, PhD**[1,2,5,6]

[1]University of Pittsburgh, Department of Surgery

[2]University of Pittsburgh, Department of Bioengineering

[3]University of Pittsburgh, Department of Orthopaedics

[4]University of Pittsburgh, Stem Cell Research Center

[5]University of Pittsburgh, McGowan Institute for Regenerative Medicine

[6]University of Pittsburgh, Center for Vascular Remodeling and Regeneration

Abstract

The success of small-diameter tissue engineered vascular grafts (TEVGs) greatly relies on an appropriate cell source and an efficient cellular delivery and carrier system. Pericytes have recently been shown to express mesenchymal stem cell features. Their relative availability and multipotentiality make them a promising candidate for TEVG applications. The objective of this study was to incorporate pericytes into a biodegradable scaffold rapidly, densely and efficiently, and to assess the efficacy of the pericyte-seeded scaffold *in vivo*. Bi-layered elastomeric poly(ester-urethane)urea scaffolds (length=10mm; inner diameter=1.3mm) were bulk seeded with 3×10^6 pericytes using a customized rotational vacuum seeding device in less than 2 min (seeding efficiency > 90%). The seeded scaffolds were cultured in spinner flasks for 2 days and then implanted into Lewis rats as aortic interposition grafts for 8 weeks. Results showed pericytes populated the porous layer of the scaffolds evenly and maintained their original phenotype after the dynamic culture. After implantation, pericyte-seeded TEVGs showed a significant higher patency rate than the unseeded control: 100% versus 38% ($p < 0.05$). Patent pericyte-seeded TEVGs revealed extensive tissue remodeling with collagen and elastin present. The remodeled tissue consisted of multiple layers of α-smooth muscle actin- and calponin-positive cells, and a von Willebrand factor-positive monolayer in the lumen. These results demonstrate the feasibility of a pericyte-based TEVG and suggest that the pericytes play a role in maintaining patency of the TEVG as an arterial conduit.

Address correspondence to: David A. Vorp, Ph.D., Professor of Surgery and Bioengineering, McGowan Institute for Regenerative Medicine, Center for Vascular Remodeling and Regeneration, 450 Technology Drive, Suite 300, Pittsburgh, PA 15219, Phone: 412-624-5319, FAX: 412-624-5363, VorpDA@upmc.edu.

Disclosures

None

Keywords

tissue engineering; vascular graft; pericyte; and rat model

Introduction

Cardiovascular disease accounts for 1 in every 2.8 deaths in the United States and costs approximately $475 billion in 2009 [1]. 56% of these deaths come from diseases of peripheral and coronary arteries, the latter resulting in 500,000 coronary artery bypass grafts (CABG) each year [1]. Together with CABG, lower limb revascularization and arteriovenous access grafts for hemodialysis account for more than 1 million vascular graft implantations per year [2]. Although autologous grafts are the gold standard for bypass procedures, they are limited by availability. Current synthetic grafts are not suitable for small-diameter (ID<6mm) vascular applications due to the acute thrombosis [3–5]. While a tissue-engineered vascular graft (TEVG), constructed by incorporating cells within a biodegradable scaffold, seems to be a possible solution to this challenge [6–8], its success greatly relies on an appropriate cell source and an efficient cellular delivery and carrier system.

Mesenchymal stem cells (MSCs) exhibiting multipotentiality and self-renewal capabilities could overcome the limitations of slow growth rate and phenotype switching with terminally-differentiated vascular cells during *in vitro* culture [9,10]. Utilization of stem cells from a human source represents a crucial step toward clinical translation of autologous TEVGs. Human adult MSCs such as bone marrow stem cells [11,12], adipose-derived stem cells [13] and endothelial progenitor cells [14] have been shown to have potential in TEVG applications. Recently, the perivascular origin of the MSCs has been shown [15–17]. Pericytes, which closely encircle endothelial cells in capillaries and microvessels [18], have been shown to be precursors of MSCs [15–17]. Their relative availability from any tissues with capillary support such as muscle and fat, as well as their multipotentiality, make pericytes a promising cell source for TEVG applications. Although differentiation toward myogenic, osteogenic, chondrogenic and adipogenic cell lineages has been demonstrated for pericytes [15,17], vasculogenic potential of pericytes remains unknown. To our knowledge, this is the first report on the use of pericytes for TEVG applications.

For those approaches that rely on cell seeding of a scaffold prior to implantation of the TEVG, few if any utilize a highly-efficient bulk-seeding process to achieve densely and uniformly distributed cells. The traditional approaches have relied on static cell culture techniques *via* pipetting the cell suspension onto the scaffold, which is associated with cell loss and uneven cell distribution [19–21]. In order to maximize the utilization of donor cells, we have developed a rotational vacuum seeding device that can efficiently incorporate a large amount of cells in a short period of time with an even distribution throughout the thickness [22,23]. The first goal of this study was to rapidly, densely and efficiently incorporate human pericytes (hPs) into a biodegradable and elastomeric scaffold and evaluate their subsequent behavior.

Autologous or allogeneic models are typically used to evaluate the performance of animal stem cell-based TEVGs. For example, TEVGs constructed from sheep endothelial progenitor cells were implanted as a carotid interposition graft in the same animal [24]. In another study, autologous bone marrow cell-seeded scaffolds were implanted to replace the inferior vena cava in dogs [25]. In one of our previous studies, biodegradable scaffolds seeded with allogeneic rat muscle derived stem cells were used as infrarenal aortic interposition grafts [26]. Although these studies showed improved patency for cellularized

TEVGs compared to their acellular counterparts, the outcome of an animal cell-based model holds minimal relevance for human cell-based TEVGs. Therefore, the second goal of this study was to assess the performance of the hP-seeded scaffold as an aortic interposition TEVG in a xenogeneic rat model.

Methods

Fabrication and Characterization of ES-TIPS PEUU scaffolds

Bi-layered, elastomeric and tubular scaffolds (1.3 mm inner diameter) with an inner porous layer and an external fibrous layer were fabricated from poly(ester-urethane)urea (PEUU). PEUU was synthesized from polycaprolactone diol and 1,4-diisocyanatobutane with a putrescine chain extender [27]. The inner PEUU tubular scaffolds were fabricated by thermally induced phase separation (TIPS) method [28]. Subsequently, PEUU nanofibers were directly deposited on the external surface of TIPS tubular scaffolds by electrospinning (ES) to obtain ES-TIPS bi-layered scaffolds [2].

The morphology of ES-TIPS PEUU scaffolds was assessed under scanning electron microscopy (SEM, JSM-6330F, JEOL, Japan) after platinum coating. The porous structure of the scaffold was imaged using micro-computed tomography (micro-CT, VivaCT40, SCANCO Medical, Brüttisellen, Switzerland). Scan settings were E=45 kVp, I=177 μA, integration time of 300 ms with 3× frame averaging, 10 μm isotropic voxel resolution, and a scan distance of 2.15 mm. Planar slice images were reconstructed from the isotropic slice data, and compiled to generate a 3-D image using a low threshold value.

Static compliance was calculated from pressure-diameter data collected *via* a pressure transducer (Model TJE, Honeywell-Sensotec Co., Columbus, OH) and He-Ne laster micrometer (Beta LaserMike, Dayton, OH) as previously described [2]. Tensile tests were carried out to measure the ultimate tensile stress (UTS) of the scaffold in the circumferential direction using an Instron 5543A testing machine (Norwood MA) and ring specimens, following a similar experimental protocol as previously reported [29]. Burst pressure was estimated from UTS as reported previously [23,30] by rearranging the law of Laplace (*i.e.* burst pressure= material yield stress × thickness/radius).

Human Pericyte (hP) Isolation and Culture

The use of hPs was in compliance with the Institutional Review Board at the University of Pittsburgh. Pericytes derived from human skeletal muscle were isolated and cultured as previously described [31,32]. Briefly, skeletal muscle was carefully separated from fat and macro vasculature then minced into small pieces. The muscle was then incubated for 45 min at 37 °C in medium containing DMEM high glucose (Gibco), 20% FBS (Gibco), 1% Penicillin-Streptomycin (PS) (Gibco) and complemented by 0.5 mg/ml of each collagenases type I, II, and IV. The resulting cell suspension was filtered to eliminate all debris. After rinsing, cells were FACS-sorted according to positive expression for CD146, NG2 (a proteoglycan associated with pericytes during vascular morphogenesis) and PDGF-Rβ, and to the absence of hematopoietic (CD45), endothelial (CD34), and myogenic (CD56) cell markers. The dead cells were excluded by FACS *via* propidium iodure staining. Sorted pericytes were seeded at 2×10^4 cells/cm^2 in endothelial cell growth medium 2 (EGM-2, Cambrex Bioscience) and cultured at 37 °C for 2 weeks in plates coated with 0.2 % gelatin (Calbiochem). Pericytes were trypsinized once a week and cultured at 1:3 dilution (from passage 1 to 5) then at 1:10 (after passage 5). Except for the first passage, all pericytes were cultured in DMEM/FBS/PS proliferation medium in uncoated flasks to maintain their original phenotype. Pericytes between passages 9 and 11 were used for all experiments.

Incorporation of Cells into the Scaffolds

The hP suspension was seeded into the ES-TIPS PEUU scaffolds *via* a previously-described vacuum rotational seeding device [22]. In brief, the scaffold was connected to two coaxial stainless steel tees inside an airtight chamber. The chamber was connected to house vacuum to maintain a negative and constant pressure (−130 mmHg), which induced transmural flow of the cell suspension across the scaffold. A syringe pump infused the cell suspension (1×10^6 cells/mL) at 2.5 mL/min into the manually rotating scaffold to reach 3×10^6 cells per scaffold within less than 2 min, resulting in a scaffold with uniformly distributed cells. Seeded scaffolds were immediately put into static culture for 3 hours, which is sufficient for cellular attachment [23]. Scaffolds were then transferred to a spinner flask with 200 mL medium at 15 rpm stirring for 2 days of culture, after which it was implanted into the rat.

Scaffolds were observed under SEM immediately after seeding. The seeded scaffolds after 2 days' dynamic culture were further assessed for histology (H&E), cellular distribution (F-actin and nuclear staining), and attachment (SEM). For F-actin staining, cryosections were permeabilized (0.1 % Triton) for 30 min, blocked (2 % BSA) for 30 min and then incubated with Alexa 488-conjugated phalloidin (1:500, Sigma) for 1 hour.

Implantation of the hP-Seeded Scaffolds into the Rat Model

All rat studies were conducted in compliance with the Institutional Animal Care and Use Committee of the University of Pittsburgh. hP-seeded scaffolds (n=7) and unseeded scaffolds (n=8) were implanted end-to-end into the abdominal aorta of female Lewis rats (200–300 g, Charles River, PA) as previously described [26]. Briefly, rats were anesthetized with isofluorane and ketamine. Before skin incision, one dose of cefuroxime (100 mg/kg) as antibiotic was administered intramuscularly for prophylaxis of surgical infections. The skin of the anterior abdominal wall was aseptically prepped with povidone-iodine solution. A midline laparotomy incision was made and the abdominal aorta exposed. Microclamps were applied to the infrarenal aorta and both common iliac arteries. An interposition aortic hP-seeded scaffold was sutured to replace the native aorta in an end-to-end anastomotic pattern with 10.0 prolene. After the scaffold was anastomosed, the clamps were released and patency of the scaffold verified by direct observation. The muscle layer and skin were then closed with 3-0 polyglactin absorbable suture. The rats were observed in the surgical suite until fully recovered from the anesthesia, then returned to the housing area. The first 3 days after surgery, buprenorphine (0.5 mg/kg) and cefuroxime (100 mg/kg) were administered intramuscularly. Antiplatelet therapy was started after the surgery with aspirin and dipyridamole. At the end of 8 weeks, the rats were anesthetized with 5% isofluorane followed by lethal intracardiac injection of heparin/KCl (40 IU of heparin in 5 ml of KCl)

Patency Assessment

Assessment of patency at the end of the 8 week implant duration was performed *via* angiography. Briefly, rats were euthanized and the thoracic descending arteries were immediately exposed and cannulated with a 22G Angiocath (BD, Sandy, UT). Rats were then put inside a dynamic angiography system (OEC 9800 Plus, GE Healthcare, Piscataway, NJ). Iodine contrast medium (Renografin-60, Bracco Diagnostics, Princeton, NJ) was manually infused through the Angiocath and the angiogram was recorded for patency verification.

Gross Pathology

After angiography, TEVGs were explanted along with a small length of the host aorta at both ends and placed in saline. To assess gross pathology, the explanted TEVGs were observed under a dissecting stereo microscope (SMZ660, Nikon Instruments Inc., Melville,

NY). TEVGs were subsequently cut into several short segments for the various endpoint studies as described below.

SEM Analysis

To further evaluate the morphology of the luminal surface, separate segments of TEVGs were cut along the longitudinal direction, laid flat, fixed in 2.5% glutaraldehyde solution for 30 min and then subjected to serial dehydration in ethanol. After platinum coating, the luminal morphology of the TEVGs was observed under SEM (JSM-6330F, JEOL Japan).

Histology and Morphometric Analysis

Separated segments of TEVGs and the native rat aorta were fixed in 4% paraformaldehyde, washed in PBS and then immersed into 30% sucrose solution overnight at 4 °C before paraffin embedding and sectioning. Hematoxylin & eosin (H&E), Masson's trichrome stain and Verhoeff-van Gieson stain were performed following standard histological protocols. Histological slides were imaged under bright field (Eclipse E800, Nikon Instruments Inc., Melville, NY) provided with a digital color CCD camera (Model 2.3.1, Diagnostic Instruments Inc., Sterling Heights, MI).

Morphometric analysis was carried out for pre-implanted scaffolds (n=9) and explanted hP-seeded TEVGs (n=7) but not for unseeded control explants as most of them were obstructed. For each TEVG or scaffold, one 8 μm section of Masson's trichrome image was taken under epifluorescent microscope (Nikon Eclipse E800) at the magnification of 4×. Images were stitched using ImageJ software (National Institutes of Health, MD) to yield an entire cross-section. Three measurements were taken for each scaffold and then averaged inner (D_i) and outer diameters (D_o) were calculated from the luminal (A_i) and total area (A_o) respectively. The total wall thickness (t_T) was calculated as $\frac{D_o - D_i}{2}$. Due to the distinct edge between the remodeled tissue and remaining TIPS layer in the histology image, the area enclosed by the edge of remodeled tissue was measured (A_{re}) and corresponding diameter (D_{re}) calculated. Then thickness of the remodeled tissue (t_{re}) was calculated as $\frac{D_{re} - D_i}{2}$. The area ratio of remodeled tissue, reflecting the degree of scaffold remodeling, was defined as the percentage of total wall area occupied by the remodeled tissue calculated as $\frac{A_{re} - A_i}{A_o - A_i} \times 100\%$.

Imunohistochemistry

Cryosections of the TEVGs and native rat aorta were permeabilized in 0.1 % Triton for 30 min and then blocked in 2% BSA for another 30 min. The cryosections were then incubated for 1 hour at room temperature with mouse anti-human primary antibodies to α-smooth muscle actin (SMA, 1:500, Sigma), h1-calponin (CALP, 1:200, Dako), and myosin heavy chain (MHC, 1:400, Abcam) to detect SMCs, and with rabbit anti-human von Willebrand factor (vWF, 1:100, Dako) to detect endothelial cells (ECs). After washing, a mixture of Alexa 488-labeled donkey-anti rabbit and Cy3-labeled donkey-anti mouse IgG was added and incubated for another 1 hour at room temperature. After counterstaining in DAPI and mounting in gelvatol, slides were observed under epifluorescence (Nikon Eclipse E800).

Fluorescent in Situ Hybridization (FISH)

Human-specific pan-centromeric and chromosome 12 probes were used to study the engraftment of hPs in explanted TEVGs. The probes were hybridized onto the cryosections of the hP-seeded TEVGs and human muscle fibers (positive control). In brief, sections were

serially dehydrated in ethanol solutions and air dried. A direct rhodamine-labeled fluorescent all-human centromere satellite probe (Qbiogene/MP Biomedicals, Solon, Ohio) or biotin-conjugated human chromosome 12 probe (ID LABS INC, London, ON, Canada) was added onto the sections following the manufacturer's protocols. Sections were covered by size-matched plastic coverslips, sealed with rubber cement (Elmer's) to prevent probe evaporation then co-denatured for 5 min at 75 °C. Sections were then incubated in a humid chamber overnight at 37 °C for the hybridization of the probes. Post-hybridization washes for the centromere probe were performed first in PBS at room temperature, and then in 0.5% SSC with 0.1% SDS for 5 min at 65 °C, followed again by a PBS wash. Post-hybridization washes for the chromosome 12 probe were performed first in 2×SSC with 0.1% Igepal (Sigma), followed by 0.4×SSC with 0.3% Igepal for 2 min at 73 °C, and then in 2×SSC with 0.1% Igepal for 5 min at room temperature. Cy3-conjugated avidin was used to visualize the chromosome 12 probe. Nuclei were counterstained with DAPI (1:2000, Molecular Probes). The slides were observed under epifluorescence (Nikon Eclipse E800).

Statistical Analysis

All quantitative values are averaged and expressed as mean ± standard deviation. Student's t-test (two-sample unequal variance) was carried out for morphometric analysis. Fisher's exact test for nonparametric variables was used to compare patency rate between the seeded and unseeded TEVGs. *P values* < 0.05 were considered significant.

Results

ES-TIPS PEUU Scaffold Characterization

Under both SEM (Fig. 1) and micro-CT (Fig. 2), the ES-TIPS PEUU scaffold displayed a bi-layered structure: *i.e*. a thick, high-porosity, internal layer, and a thin, dense, fibrous, external layer. The TIPS layer thickness was approximately 400 μm with a pore size of approximately 50 μm. The ES layer thickness was approximately 70 μm with a pore size of approximately 5 μm. The diameter of the ES nanofibers ranges between 500–900 nm.

The ES-TIPS PEUU scaffold had a compliance value of 2.4 ± 1.1%/100 mmHg (n=7), which is lower than that of the native rat aorta (12.1 ± 1.7%/100 mmHg) and close to that of the native rat vena cava (4.9 ± 0.8 %/100 mmHg). The measured UTS of the scaffold was 0.8 ± 0.2 MPa (n=6). Burst pressure was estimated to be 4462 ± 1201 mmHg (n=6).

In Vitro hP Seeding and Culture

The open and interconnected pores of the TIPS layer were occupied by cells after seeding (Fig. 3). The seeding efficiency was above 90%. While most cells were still rounded up (Fig. 3C), some cells were spread on the surfaces of the pores (Fig. 3D).

Following 2 days of dynamic culture in the spinner flask, hPs populated the whole TIPS layer of the scaffolds, with a uniform circumferential and radial distribution (Fig. 4). Under SEM observation, hPs were found to completely fill some pores (Fig. 4B). hPs maintained their original phenotype of expressing α-SMA, CD 146 and failing to express CD34 and other EC markers after the dynamic culture (data not shown).

In Vivo Implantation

All scaffolds showed good suturability and pliability which allowed for effective end-to-end anastomosis. The angiograms performed to evaluate the patency rate showed that all 7 (100%) hP-seeded TEVGs (Fig. 5A) but only 3 out of 8 (38%) unseeded TEVGs (Fig. 5E) were patent while the rest were obstructed. There was a significant difference in patency rate between the two groups (p=0.026). All patent hP-seeded TEVGs displayed a tissue-like

appearance with clear remodeling of the scaffold and without visible signs of infection or scar tissue formation (Fig. 5B–5D). The lumen of the patent TEVGs was smooth and shiny without thrombosis formation (Fig. 5B). Patent TEVGs also exhibited size matching with the native aorta at the anastomosis sites (Fig. 5C). Obstructed unseeded controls showed overgrowth of tissue in the lumen, suggestive of intimal hyperplasia (Fig. 5F and 5H).

SEM analysis of the luminal surface of the patent TEVGs revealed a smooth transition from the native aorta to the TEVGs (Fig. 6B) and suggested coverage of an endothelial-like confluent cells (Fig. 6C). The unseeded controls showed platelet aggregation on the luminal surface (Fig. 6D).

Histological analysis demonstrated tissue remodeling in the TIPS layer enriched with both collagen and elastin (Fig. 7A–7F). The ES layer appeared intact without cell infiltration (Fig. 7D–7F). Similar histology results were observed in the native rat aorta (Fig. 7J–7L). As expected, the unseeded controls displayed obstructed lumen (Fig. 7G–7I).

Morphometric analysis of the patent hP-seeded TEVGs showed a significantly increased inner diameter (D_i) and outer diameter (D_o) ($P < 0.05$) but similar wall thickness (t_T) compared with the pre-implanted scaffolds (Table 1).

Immunohistochemical analysis showed that the remodeled tissue noticed in Fig. 7A–7F consisted of multiple layers of α-SMA- and h1-calponin-positive cells, suggesting the contractile SMC phenotype, and a monolayer of vWF-positive cells, suggesting ECs on the luminal surface (Fig. 8A–8C). Similar cellular compositions were observed in the native rat aorta (Fig. 8D–8F), although MHC-positive cells were not found in the TEVGs, suggesting the regenerated SMCs were not of a fully-contractile phenotype at 8 weeks. It is possible that with longer implantation duration, SMCs might switch to more mature contractile phenotype when exposed to continuous cyclic stretching caused by systemic circulation. None of these vascular markers were observed in the unseeded controls (data not shown).

Fluorescent in situ hybridization (FISH) results showed red signal co-localized with blue nuclei in the positive control (human muscle sections) for both human-specific probes (Fig. 9A and 9C), indicating the efficiency of probe hybridization to human nuclei was very high. However, almost no positive staining co-localized with nuclei was visualized on the explanted hP-seeded TEVG (Fig. 9B and 9D), suggesting a scarcity of human cells and presence of host rat cells.

Discussion

In this study, we have shown that bi-layered PEUU scaffold efficiently seeded with human pericytes, dynamically cultured for 2 days, and implanted *in vivo* remodeled into a patent small diameter arterial graft. The hP-seeded TEVGs showed a significantly higher patency rate compared with the unseeded counterparts, suggesting that pericytes play a role in maintaining patency of the TEVGs.

Generating TEVGs from human cells represents a critical step towards clinical translation of vascular tissue engineering. Niklason *et al*., fabricated hTEVGs using genetically-modified terminally-differentiated SMCs and ECs with telomerase expression isolated from elderly patients to overcome the limited replicative capacity of adult somatic cells [33]. McAllister *et al*., also reported clinical studies of implanting autologous human TEVGs engineered from human skin fibroblasts and venous endothelial cells as arteriovenous shunts [34]. Although both approaches represent a breakthrough, the use of terminally-differentiated cells results in a long fabrication time and lack of off-the-shelf capability of TEVG, which might be overcome by the use of human multipotent stem cells. We have shown here that

tubular biodegradable scaffolds seeded quickly and efficiently with hPs and pre-cultured for 2 days resulted in SMC- and EC- populated conduits *in vivo*. These results suggest that pericytes and other MSCs might be used as an alternative to terminally-differentiated vascular cells for TEVG application.

Although most reports of xenogeneic implantation use either immune-suppressed animals or immunodeficient rodents (*i.e.*, SCID mice or nude rat) [11,35,36], we used the immune-competent Lewis rat. No gross inflammation response to the hP-seeded scaffolds was observed (Fig. 5–8). One possible explanation for this is that pericytes, as progenitors of MSCs [16,17], may secrete anti-inflammatory cytokines, resulting in lack of immune clearance [37]. Immunosuppression by human pericytes is currently under study with preliminary results supporting this possibility.

The precise role of hPs in TEVG remodeling and functionality is unknown. It is possible that they provide acute anti-thrombogenicity while modulating the recruitment of host cells (e.g., from the anastomosis, circulating progenitor cells and/or hematopoietic/immune cells), which then directly participate in the remodeling process. This possibility is supported by a report that human bone marrow MSCs seeded on nanofibrous vascular grafts provide anti-thrombogenicity but majority of the MSCs had short-term (less than 7 days) engraftment in a rat model [11]. Similarly, it was recently shown that seeded human bone marrow MSCs enhance the recruitment of host rat monocytes to the TEVGs which participated in the remodeling, with the seeded cells not detectable within a few days of implantation [21].

The observed dilation of the hP-seeded TEVGs represents a limitation of the work (Table 1). Since no dilation was observed for the rat stem cell-seeded scaffolds in our previous work [26], dilation is likely due to distension damage incurred by the scaffold upon *in vitro* seeding, or accelerated mechanical degradation of the scaffolds *in vivo*. hPs are three- to five-times larger than rat cells. Using the same seeding protocol (*i.e.*, flow rate and driving pressure of cell suspension infusion) as in our previous rat TEVG studies resulted in high resistance and dilation of the scaffold during seeding, which may have caused irreversible structural damage. Even a moderate xenogeneic host-foreign body response could cause accelerated degradation of the PEUU scaffolds through hydrolysis and macrophage phagocytosis and result in dilation. Supporting this possibility, we observed that hP-seeded scaffolds display more profound remodeling than the rat stem cell-seeded counterparts for the same implantation duration (data not shown). Another limitation of current work is that the burst pressure was only estimated *via* a simplified analytical expression (Laplace) due to the small size of the scaffolds, which might be overestimated by over 50% according to the report from Cytograft® [30].

Conclusions

A biodegradable, tubular scaffold densely and uniformly seeded with human pericytes, then cultured for 2 days in a spinner flask, appears to be a promising new, small diameter tissue engineered vascular graft. After implantation, pericyte-seeded TEVGs showed a higher patency rate than the unseeded control. The pericytes play a key, yet unknown role in remodeling the scaffold into a patent TEVG demonstrating tissue-like appearance. Future work is needed in order to perform more rigorous engraftment studies, functional tests, longer-term implantation, and cell tracking along the implantation duration.

Acknowledgments

The authors would like to acknowledge the funding support from NIH R01 HL069368 to Drs. Wagner and Vorp, and AHA 0525585U to Dr. Nieponice. We thank the Center for Biological Imaging, and the staffs of the McGowan animal facility and histology lab for their technical help.

References

1. Lloyd-Jones D, Adams RJ, Brown TM, Carnethon M, Dai S, et al. WRITING GROUP MEMBERS. Heart Disease and Stroke Statistics--2010 Update: A Report From the American Heart Association. Circulation. 2010; 121(7):e46–215. [PubMed: 20019324]
2. Soletti L, Hong Y, Guan J, Stankus JJ, El-Kurdi MS, Wagner WR, et al. A bilayered elastomeric scaffold for tissue engineering of small diameter vascular grafts. Acta Biomater. 2010; 6(1):110–22. [PubMed: 19540370]
3. Matsuda T. Recent progress of vascular graft engineering in Japan. Artif Organs. 2004; 28(1):64–71. [PubMed: 14720291]
4. Niklason, LESM. Small-Diameter Vascular Grafts. In: Atala, ALRP., editor. Methods of Tissue Engineering. Academic Press; San Diego: 2002. p. 905
5. Seal BL, Otero TC, Panitch A. Polymeric biomaterials for tissue and organ regeneration. Mat Sci Eng R. 2001; 34(4–5):147–230.
6. Kakisis JD, Liapis CD, Breuer C, Sumpio BE. Artificial blood vessel: the Holy Grail of peripheral vascular surgery. J Vasc Surg. 2005; 41(2):349–54. [PubMed: 15768021]
7. Thomas AC, Campbell GR, Campbell JH. Advances in vascular tissue engineering. Cardiovasc Pathol. 2003; 12(5):271–6. [PubMed: 14507577]
8. Xue L, Greisler HP. Biomaterials in the development and future of vascular grafts. J Vasc Surg. 2003; 37(2):472–80. [PubMed: 12563226]
9. Caplan AI. Adult mesenchymal stem cells for tissue engineering versus regenerative medicine. J Cell Physiol. 2007; 213(2):341–7. [PubMed: 17620285]
10. Eberli, D.; Atala, A. Methods in Enzymology. Vol. 420. Elsevier Academic Press Inc; San Diego: 2006. Tissue engineering using adult stem cells. Stem Cell Tools and Other Experimental Protocols; p. 287-302.
11. Hashi CK, Zhu YQ, Yang GY, Young WL, Hsiao BS, Wang K, et al. Antithrombogenic property of bone marrow mesenchymal stem cells in nanofibrous vascular grafts. P Natl Acad Sci USA. 2007; 104(29):11915–20.
12. Hibino N, McGillicuddy E, Matsumura G, Ichihara Y, Naito Y, Breuer C, et al. Late-term results of tissue-engineered vascular grafts in humans. J Thorac Cardiovasc Surg. 2010; 139(2):431–6. 36 e1–2. [PubMed: 20106404]
13. DiMuzio P, Tulenko T. Tissue engineering applications to vascular bypass graft development: the use of adipose-derived stem cells. J Vasc Surg. 2007; 45 (Suppl A):A99–103. [PubMed: 17544030]
14. de Mel A, Punshon G, Ramesh B, Sarkar S, Darbyshire A, Hamilton G, et al. In situ endothelialization potential of a biofunctionalised nanocomposite biomaterial-based small diameter bypass graft. Biomed Mater Eng. 2009; 19(4–5):317–31. [PubMed: 20042799]
15. Dellavalle A, Sampaolesi M, Tonlorenzi R, Tagliafico E, Sacchetti B, Perani L, et al. Pericytes of human skeletal muscle are myogenic precursors distinct from satellite cells. Nat Cell Biol. 2007; 9(3):255–67. [PubMed: 17293855]
16. Caplan AI. All MSCs are pericytes? Cell Stem Cell. 2008; 3(3):229–30. [PubMed: 18786406]
17. Crisan M, Yap S, Casteilla L, Chen CW, Corselli M, Park TS, et al. A perivascular origin for mesenchymal stem cells in multiple human organs. Cell Stem Cell. 2008; 3(3):301–13. [PubMed: 18786417]
18. Shepro D, Morel NM. Pericyte physiology. FASEB J. 1993; 7(11):1031–8. [PubMed: 8370472]
19. Niklason LE, Abbott W, Gao J, Klagges B, Hirschi KK, Ulubayram K, et al. Morphologic and mechanical characteristics of engineered bovine arteries. J Vasc Surg. 2001; 33(3):628–38. [PubMed: 11241137]
20. Matsumura G, Miyagawa-Tomita S, Shin'oka T, Ikada Y, Kurosawa H. First evidence that bone marrow cells contribute to the construction of tissue-engineered vascular autografts in vivo. Circulation. 2003; 108(14):1729–34. [PubMed: 12963635]
21. Roh JD, Sawh-Martinez R, Brennan MP, Jay SM, Devine L, Rao DA, et al. Tissue-engineered vascular grafts transform into mature blood vessels via an inflammation-mediated process of vascular remodeling. Proc Natl Acad Sci U S A. 2010; 107(10):4669–74. [PubMed: 20207947]

22. Soletti L, Nieponice A, Guan J, Stankus JJ, Wagner WR, Vorp DA. A seeding device for tissue engineered tubular structures. Biomaterials. 2006; 27(28):4863–70. [PubMed: 16765436]
23. Nieponice A, Soletti L, Guan J, Deasy BM, Huard J, Wagner WR, et al. Development of a tissue-engineered vascular graft combining a biodegradable scaffold, muscle-derived stem cells and a rotational vacuum seeding technique. Biomaterials. 2008; 29(7):825–33. [PubMed: 18035412]
24. Kaushal S, Amiel GE, Guleserian KJ, Shapira OM, Perry T, Sutherland FW, et al. Functional small-diameter neovessels created using endothelial progenitor cells expanded ex vivo. Nat Med. 2001; 7(9):1035–40. [PubMed: 11533707]
25. Hibino N, Shin'oka T, Matsumura G, Ikada Y, Kurosawa H. The tissue-engineered vascular graft using bone marrow without culture. J Thorac Cardiov Sur. 2005; 129(5):1064–70.
26. Nieponice A, Soletti L, Guan J, Hong Y, Gharaibeh B, Maul TM, et al. In vivo assessment of a tissue-engineered vascular graft combining a biodegradable elastomeric scaffold and muscle-derived stem cells in a rat model. Tissue Eng Part A. 2010; 16(4):1215–23. [PubMed: 19895206]
27. Guan J, Sacks MS, Beckman EJ, Wagner WR. Synthesis, characterization, and cytocompatibility of elastomeric, biodegradable poly(ester-urethane)ureas based on poly(caprolactone) and putrescine. J Biomed Mater Res. 2002; 61(3):493–503. [PubMed: 12115475]
28. Guan J, Fujimoto KL, Sacks MS, Wagner WR. Preparation and characterization of highly porous, biodegradable polyurethane scaffolds for soft tissue applications. Biomaterials. 2005; 26(18): 3961–71. [PubMed: 15626443]
29. Stankus JJ, Soletti L, Fujimoto K, Hong Y, Vorp DA, Wagner WR. Fabrication of cell microintegrated blood vessel constructs through electrohydrodynamic atomization. Biomaterials. 2007; 28(17):2738–46. [PubMed: 17337048]
30. Konig G, McAllister TN, Dusserre N, Garrido SA, Iyican C, Marini A, et al. Mechanical properties of completely autologous human tissue engineered blood vessels compared to human saphenous vein and mammary artery. Biomaterials. 2009; 30(8):1542–50. [PubMed: 19111338]
31. Crisan M, Deasy B, Gavina M, Zheng B, Huard J, Lazzari L, et al. Purification and long-term culture of multipotent progenitor cells affiliated with the walls of human blood vessels: myoendothelial cells and pericytes. Methods Cell Biol. 2008; 86:295–309. [PubMed: 18442653]
32. Crisan M, Huard J, Zheng B, Sun B, Yap S, Logar A, et al. Purification and culture of human blood vessel-associated progenitor cells. Curr Protoc Stem Cell Biol. 2008; Chapter 2(Unit 2B 2 1-2B 2 13)
33. Poh M, Boyer M, Solan A, Dahl SL, Pedrotty D, Banik SS, et al. Blood vessels engineered from human cells. Lancet. 2005; 365(9477):2122–4. [PubMed: 15964449]
34. McAllister TN, Maruszewski M, Garrido SA, Wystrychowski W, Dusserre N, Marini A, et al. Effectiveness of haemodialysis access with an autologous tissue-engineered vascular graft: a multicentre cohort study. Lancet. 2009; 373(9673):1440–6. [PubMed: 19394535]
35. Nelson GN, Mirensky T, Brennan MP, Roh JD, Yi T, Wang Y, et al. Functional small-diameter human tissue-engineered arterial grafts in an immunodeficient mouse model: preliminary findings. Arch Surg. 2008; 143(5):488–94. [PubMed: 18490559]
36. Lopez-Soler RI, Brennan MP, Goyal A, Wang Y, Fong P, Tellides G, et al. Development of a mouse model for evaluation of small diameter vascular grafts. J Surg Res. 2007; 139(1):1–6. [PubMed: 17336332]
37. Aggarwal S, Pittenger MF. Human mesenchymal stem cells modulate allogeneic immune cell responses. Blood. 2005; 105(4):1815–22. [PubMed: 15494428]

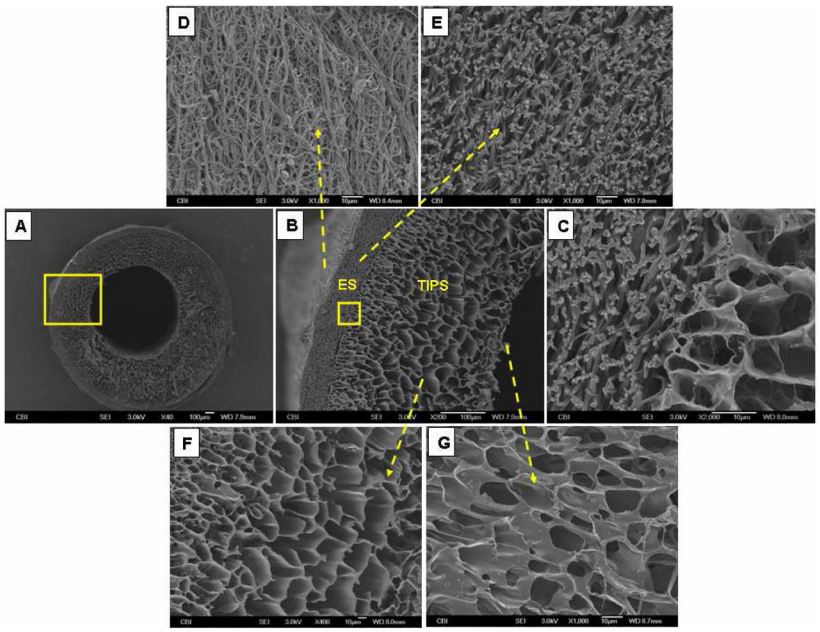

Fig. 1.

Representative SEM micrographs of the ES-TIPS PEUU scaffold (ID 1.3 mm). (A) Whole cross-section; (B) higher magnification of the close-up in (A); (C) higher magnification of the close-up in (B), showing adherence between the ES and TIPS layer; (D) outer surface of the ES layer; (E) cross-section of the ES layer; (F) cross-section of the TIPS layer; (G) inner surface of the TIPS layer.

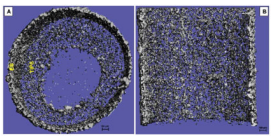

Fig. 2.
Representative micro-CT images of the ES-TIPS PEUU scaffold. Cross-section in (A) radial plane and (B) longitudinal plane.

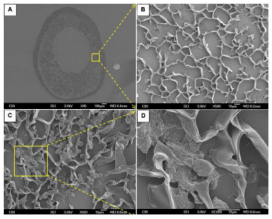

Fig. 3.
Representative SEM micrographs of a thin-section (thickness: 10 μm) of the ES-TIPS PEUU scaffold (A and B) before and (C and D) after cell seeding. (A) Whole cross-section; (B) higher magnification of the close-up in (A), showing TIPS layer before cell seeding; (C) TIPS layers after cell seeding; (D) higher magnification of the close-up in (C).

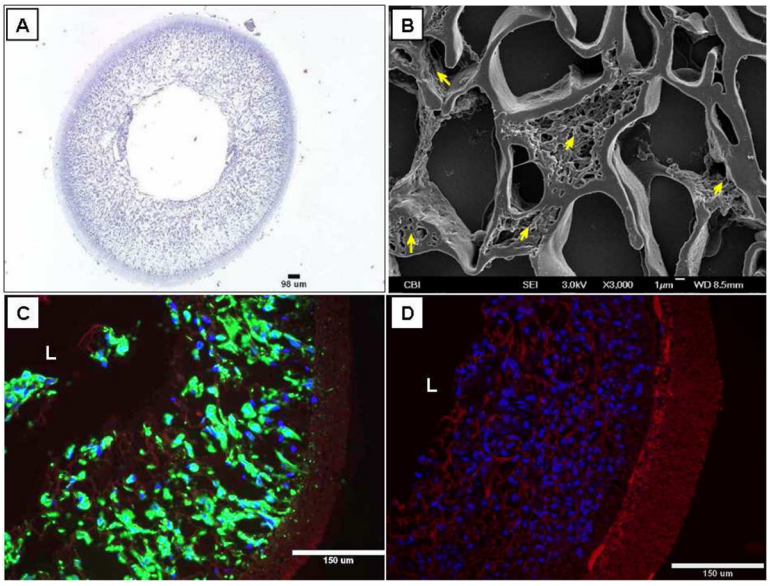

Fig. 4.

Characterizations of the pre-implanted hP-seeded ES-TIPS PEUU scaffolds after dynamic culture. (A) H&E staining; (B) SEM (arrows=cells); (C) F-actin staining (red=scaffold; blue=nuclei; green=F-actin), and (D) nuclear staining (red= scaffold; blue=nuclei). “L” indicates lumen.

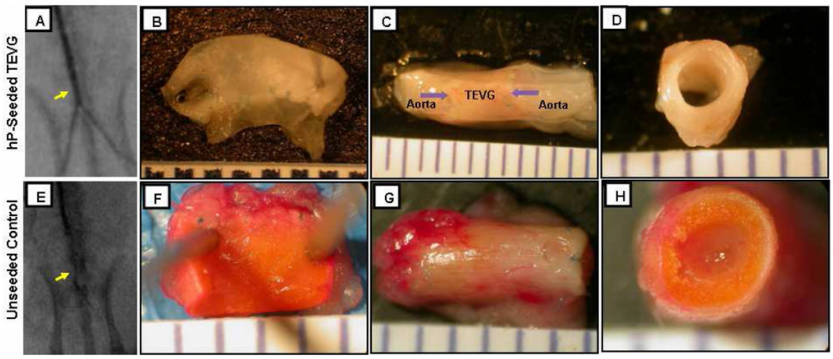

Fig. 5.

Representative angiographic and gross pathology images of the (A-D) hP-seeded TEVG and (E-H) unseeded control. (A and E) Angiographic images (arrow=implant); (B and F) macroscopic images of the lumen, (C and G) entire length, and (D and H) whole cross-section. Arrows in (C) indicate anastomosis marked by suture lines.

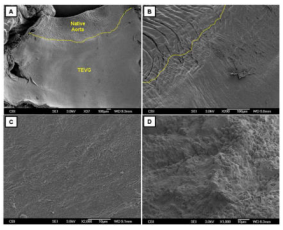

Fig. 6.

Representative SEM micrographs of the (A-C) hP-seeded TEVG and (D) unseeded control. (A) Luminal surface of the hP-seeded TEVG with adjacent rat aorta; (B) higher magnification of the anastomosis site between the rat aorta and the hP-seeded TEVG; (C) higher magnification of the luminal surface of the hP-seeded TEVG; (D) luminal surface of the unseeded control, showing the platelet aggregation. Anastomosis is manually depicted in (A and B).

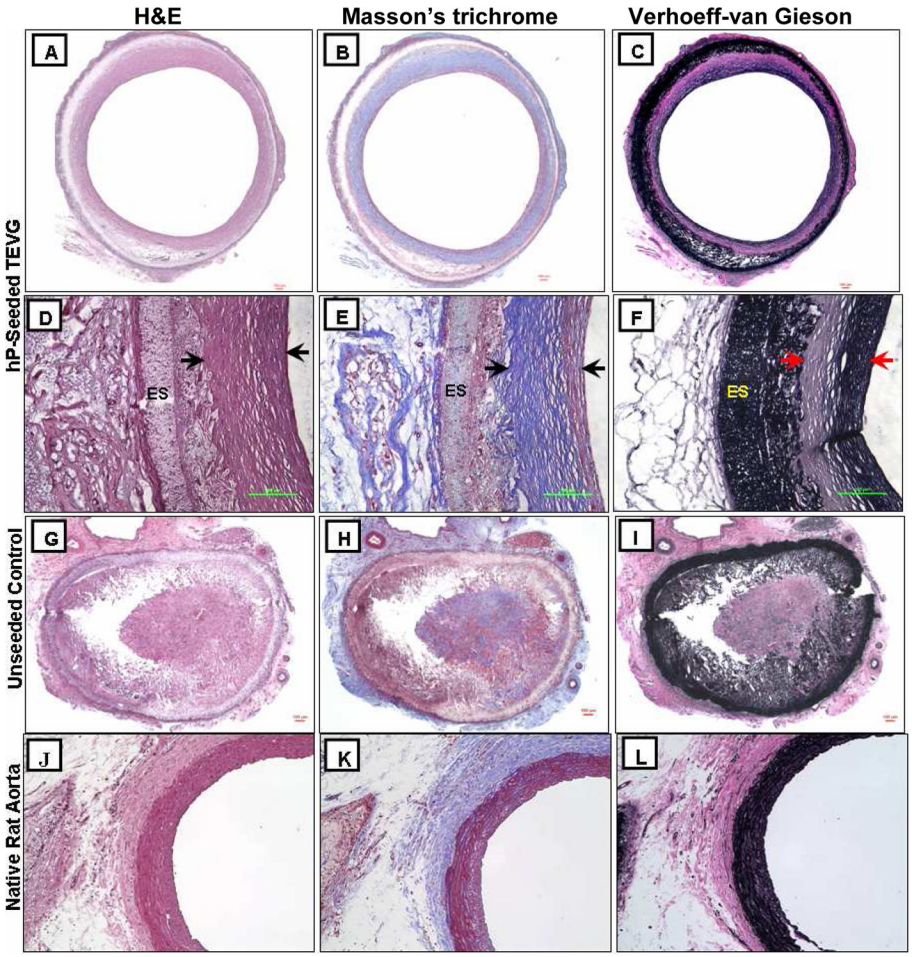

Fig. 7.

Representative histological images of the (A-F) hP-seeded TEVG, (G-I) unseeded control, and (J-L) native rat aorta. (A, D, G and J) H&E, (B, E, H and K) Masson's trichrome, and (C, F, I and L) Verhoeff-van Gieson staining. (D-F) Higher magnification of (A-C). Arrows in (D-F) indicate the thickness of the remodeled tissue layer, while "ES" indicates the ES layer. The remaining PEUU material was unspecifically stained in black by Verhoeff-van Gieson stain in (F and I). Magnification for (A-C and G-I): ×4, (D-F): ×40, (J-L): ×20.

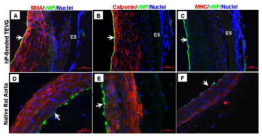

Fig. 8.

Representative immunohistochemistry images of the (A-C) hP-seeded TEVG and (D-F) native rat aorta. (A and D) α-SMA, (B and E) h1-calponin, and (C and F) myosin heavy chain (MHC) double-stained with von Willibrand factor (vWF) (red=SMA/calponin/MHC; green=vWF; blue=nuclei). Arrows indicate lumen. ES layer is indicated in (A-C), showing no cell infiltration in the ES layer.

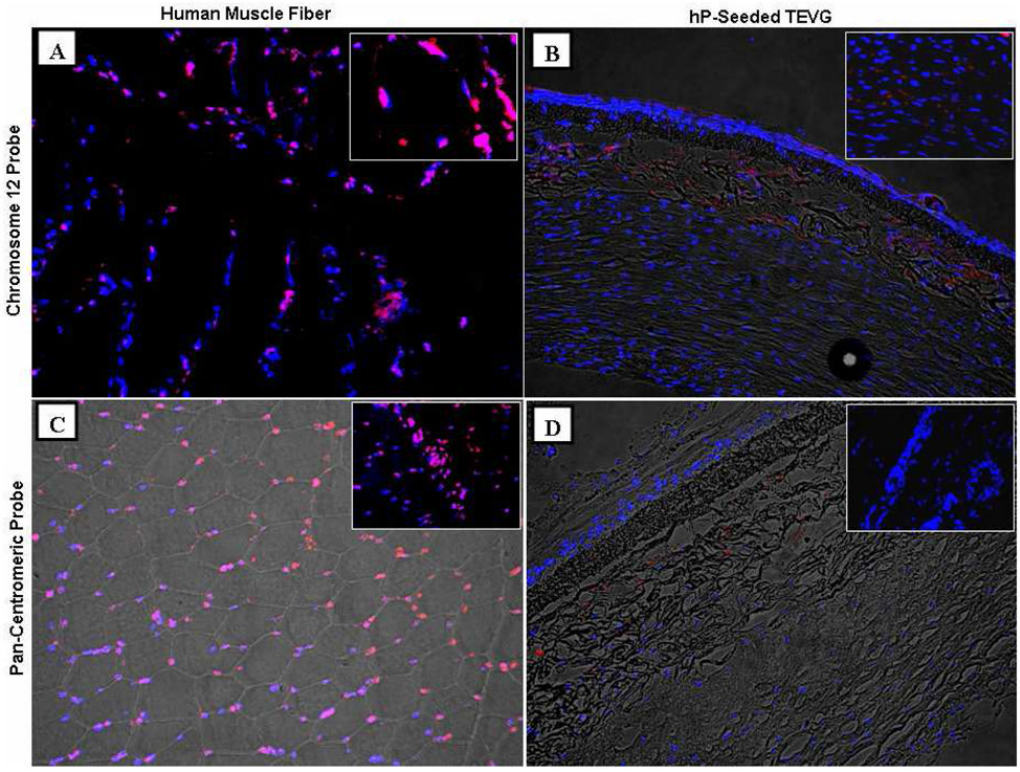

Fig. 9.

Representative fluorescent in situ hybridization (FISH) images for engraftment study. (A and B) Human-specific chromosome 12 probe, (C and D) human-specific pan-centromeric probe (red=signal; blue=nuclei). (A and C) Human muscle fiber acting as a positive control and (B and D) explanted hP-seeded TEVG. Magnified images are shown in the insets. Magnification for (A-D): ×20; insets in (A and B): ×60; insets in (C and D): ×40. Fluorescent images and bright field images are overlaid in (B, C, and D).

Table 1

Morphometric analysis results showing the inner diameter (D_i), outer diameter (D_o), total wall thickness (t_T), remodeled tissue thickness (t_{re}), and area ratio of the remodeled tissue from the explanted hP-seeded TEVGs (n=7) and pre-implanted scaffolds (n=9).

	Explanted TEVGs (n=7)	Pre-Implanted Scaffolds (n=9)
Inner Diameter (D_i) (mm)	1.89 ± 0.57 *	0.95 ± 0.08
Outer Diameter (D_o) (mm)	2.73 ± 0.53 *	1.85 ± 0.15
Total Wall Thickness (t_T) (μm)	420 ± 144	453 ± 74
Remodeled Tissue Thickness (t_{re}) (μm)	226 ± 91	n/a
Area Ratio of Remodeled Tissue	50% ± 17%	n/a

The asterisk (*) indicates a statistically significant difference from the pre-implanted scaffolds ($p < 0.05$).